Astronomy & Astrophysics manuscript no. INTEGRAL31 February 2, 2008
(DOI: will be inserted by hand later)

Systematic effects induced on IBIS detectors by background and inhomogeneity of the spatial response ⋆

L. Natalucci[1], A.J.Bird[2], A.Bazzano[1], P.Ubertini,[1], J.B.Stephen[3], R.Terrier[4], L.Lerusse[5]

[1] CNR-Istituto di Astrofisica Spaziale e Fisica Cosmica, Area Ricerca Roma 2/Tor Vergata, Via del Fosso del Cavaliere 100, 00133 Roma, Italy
e-mail: lorenzo@rm.iasf.cnr.it

[2] Department of Physics & Astronomy, University of Southampton, SO17 1BJ,U.K.

[3] CNR-Istituto di Astrofisica Spaziale e Fisica Cosmica, Area Ricerca di Bologna, Via Gobetti 101, 40100 Bologna, Italy

[4] DAPNIA, Service d'Astrophysique, CEA/Saclay, 91191 Gif-sur-Yvette Cedex, France

[5] INTEGRAL Science Data Centre, Chemin d'Ecogia 16, CH-1290 Versoix, Switzerland

Received; Accepted

Abstract. The spatial distribution of the background events may affect the source detection capability of IBIS at high energies ($\geq$ 200 keV) for both ISGRI and PICsIT layers. The observed background is found to be variable and spatially structured, and in some cases its properties strongly deviate from the expected statistical behaviour. Background correction methods are then necessary to improve the quality of the shadowgrams obtained from sources. In order to perform an efficient flat-fielding the response of the detector to both source (γ-rays) and background events is investigated using data from Monte Carlo simulations and in-flight calibration observations.

Key words. gamma-ray astronomy; detectors; background; data analysis

1. Introduction

The IBIS instrument on board *INTEGRAL* (Winkler et al. 2003) is the first large area, space born γ-ray telescope carrying a pixellated, multi-layer detector system (Ubertini et al. 2003). Due to its large aperture and large collecting area, the scientific performances are strongly dependent on background reduction. Optimal levels of background intensity and stability in time have been reached after tuning and calibration of instrumental parameters. This has been achieved during in-flight commissioning (Ubertini et al. 2003). In IBIS, different data acquisition modes working simultaneously ensure a good capability of background rejection. Important features are the selection of single and multiple events in the high energy detector (PICsIT, Labanti et al. 2003) and of multi-layer coincidence events (*Compton* mode). Furthermore, the two detector layers ISGRI (the hard X-ray detector, Lebrun et al. 2003) and PICsIT are actively shielded by a multi-module VETO system, based on one lateral and one bottom arrays of BGO blocks (Quadrini et al. 2003). ISGRI is also shielded from the diffuse hard X-ray background outside the field-of-view by a composite passive shield protecting the whole telescope from mask to detector base (see e.g. Natalucci & Caroli 1996).

The IBIS data processing software (Goldwurm et al. 2003) is capable of recovering many time varying systematic effects as telemetry losses, noisy pixels, temporary switch-off of ISGRI modules, dead time etc., which are well quantified and properly taken into account in the analysis. Once the data have been corrected for these effects we still see important spatial structures, which affect both detector layers. These are easily detected as different average count-rates in detector modules/semi-modules, enhancements at the edge of the modules and local effects induced by the readout electronics. There are several factors known to produce this inhomogeneity of the spatial response (see also Stephen et al. 2003; Terrier et al. 2003): a) a spatially dependent hadronic background component, depending on the external payload and spacecraft mass distribution; b) the efficiency of detection of

Send offprint requests to: L. Natalucci

⋆ Based on observations with INTEGRAL, an ESA project with instruments and science data centre funded by ESA member states (especially the PI countries: Denmark, France, Germany, Italy, Switzerland, Spain), Czech Republic and Poland, and with the participation of Russia and the USA.

single and multiple events, which is expected to be dependent on the detector position; c) the individual response of each detector module; d) the intrinsic response of each pixel as a function of its position, i.e. its proximity to a module, an ASIC (Application Specific Integrated Circuit) readout element and/or a dead pixel; e) variations of the performance of the VETO modules, induced especially by temperature variations. These effects are, in turn, energy dependent. Moreover a given pixel may undergo periods of unusual behaviour. For ISGRI, defective pixels including noisy elements which are switched off permanently or for a relatively short time period may induce local variations in the detector itself and even in PICsIT. PICsIT pixels have also intrinsic noise levels that could have local effects in ISGRI. PICsIT data are normally transmitted as *spectral histograms* (SI) already accumulated on board. Varying count rates of pixels can influence the local response of detectors for less than the typical SI integration time ($\approx 2150s$), and hence cannot be properly followed in PICsIT. For this reason, local corrections based on analysis of single pixel light curves cannot be always applied efficiently. Therefore, methods of flattening the images independently of the time behaviour of pixels are being studied (see Sect. 2).

The difficulty of correcting data by using maps obtained by long background exposures is mainly related to the background being variable with time, and to different systematics in the counting behaviour of pixels in ”observation” and ”background” exposures. In the following sections, an overview of the main problems related to background induced effects is given and some results are reported in more detail, especially regarding the PICsIT detector. For PICsIT, an important source of background is the excess counts caused by the decay of long-lived phosphorescence states of the CsI crystals (Hurley 1978). These counts cannot be vetoed because they give rise to single events, separated by intervals of the order of a few 10^{-5}s. However, they can be easily identified and removed in *photon by photon* data, and their spatial distribution can be separately studied (see Sect. 4). Other spatial inhomogeneity effects which are background independent are described in Sect. 3.

2. Flat-fielding methods

For IBIS, flat-fielding prior to image deconvolution (Goldwurm et al. 2001) is essential especially at high energies, as long as the size of the fluctuations in the background level, propagated through the imaging process exceed the observed celestial source intensity. The approach of applying a flat-field based on Fourier filtering is difficult, because a substantial power of the background distribution is seen at high spatial frequencies, where most of the signal from multiplexing the source counts by the coded mask is also found. An alternative approach is to characterize each pixel by averaging on pixel categories, defined on the basis of the pixel position in the detector, i.e. proximity to a module edge and/or to a noisy/dead pixel, position within an ASIC etc. This has the form of a model map applicable to a given energy band. The model is obtained from real data by measuring average count rates for each pixel category (see Fig. 1). Correction maps defined for eight standard energy bands, covering the range 0.2-6.5 MeV, have been used to subtract a background shape from the single event shadowgrams. The resulting detector image is defined by a subtraction of the model from the original image: D_{ff}=(D_{raw}-Mf)+$\langle D_{raw}\rangle$, where M is the model map and f=$\langle D_{raw}\rangle$/$\langle M\rangle$ is the ratio between average pixel values in the raw image and model map.

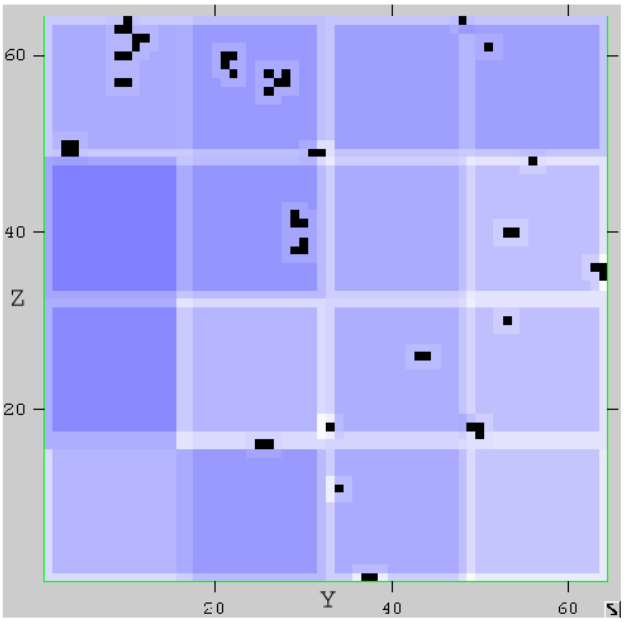

Fig. 1. Example of PICsIT model map in the energy range 190-300 keV. It shows different average levels associated to the 16 semi-modules, the *edge* pixels, and pixels surrounding *dead* pixels (the latter are shown in black). The image axes (in units of pixel index) are parallel to the spacecraft Y- and Z-axes, for which the X-axis represents the pointing direction.

The standard deviation in the pixel counts of the background subtracted shadowgram is compared to that of the original image, and a *flat-field* efficiency is evaluated as:

$$\epsilon_{ff} = (\sigma_{raw} - \sigma_{ff}) \,/\, (\sigma_{raw} - \sqrt{\langle D_{raw}\rangle})$$

We have used a model map based on the sum of 3 science windows, for a total exposure of 6450 s of an empty field observation, to flatten a series of spectral histograms obtained from a Crab exposure. In Fig. 2, the average flat-field efficiency obtained by this processing is plotted as a function of energy. We remark that in the first two energy bands, the low efficiency obtained is not intrinsic to the flat-field process, but is rather due to the effect of phosphorescence counts (see Sect. 4), causing the average deviates to be well above the Poisson statistical value. Apart from this effect, the efficiency is energy dependent.

Adding more input data in building the model maps is not found to improve the efficiency. This is probably due to the time variations in the background. Improvements to the model are currently under study, as long as more systematic effects are identified.

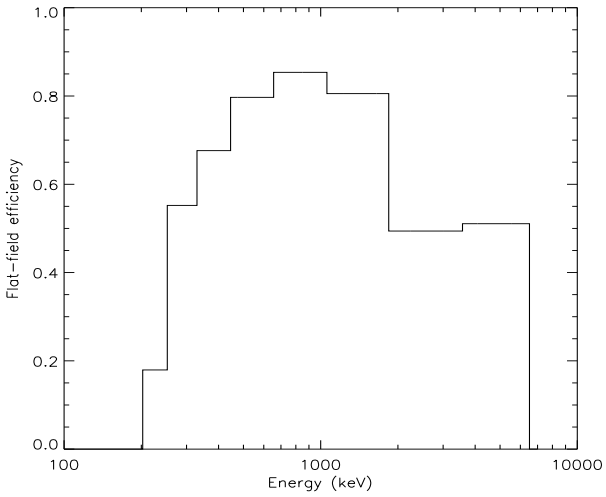

Fig. 2. Flat-field efficiency as a function of energy, for the model maps discussed in Sect.2.

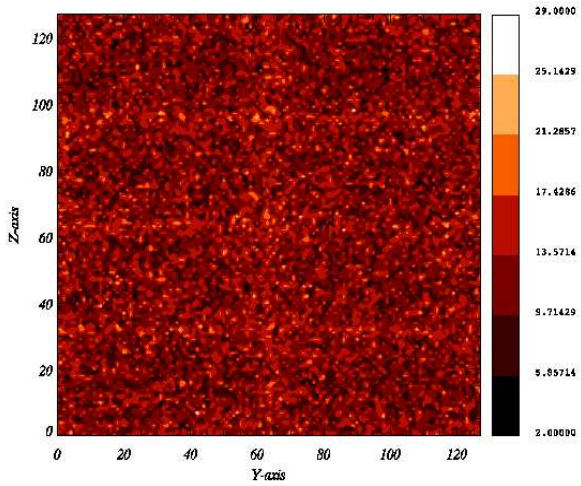

Fig. 3. Simulated map of ISGRI, as illuminated by a monochromatic source at 500 keV. The energy range is 170-400 keV. The image shows a non perfectly flat events distribution. Both axis scales refer to pixel index (0 to 127 on each side). Axes are parallel to the spacecraft Y- and Z-axes.

3. Response to γ-ray source

Besides the known effect of background non-uniformity, scattering of celestial source γ-rays associated with a non-ideal response of the event selection logic and/or non-ideal geometry of the detector can produce a non-homogeneity of the source count distribution. This component of the non-uniformity (which is intrinsically different from the background induced one) is being studied by Monte Carlo simulations using a numerical code based on a detailed geometric and mass model of the telescope, including electronics and event selection logic (Laurent et al. 2001). For this purpose, we have simulated a parallel flux of γ-rays incident on the IBIS detector with zero deg inclination, at different monochromatic photon energies and for a power law source. The efficiency and response of single pixels are considered uniform in the simulation, so inhomogeneities cannot be ascribed to their local behaviour. For a monochromatic source, it was verified that the image is perfectly uniform when selecting events under the full-energy peak. This is expected as far as there is no redistribution of the event energy in pixels other than the incidence pixel. In contrast, the count distribution shows differences, especially in the counting rate at the edge of modules, when the energy range selected covers part of the Compton continuum. This is true in particular for ISGRI (see Fig 3) and PICsIT multiple events. This non-uniformity should be ideally corrected by dividing the residual detector image after background subtraction or flat-field (see Sect. 2) by an *efficiency* map which takes into account the scattering induced effects. This is, of course, dependent on the input source spectrum. A set of reference efficiency maps are being computed for a limited set of input spectra models (based on power law or cutoff power laws) to be tested and compared. We consider, however, that correcting real data using a non-uniformity model of the source illumination is expected to be of secondary importance compared to an efficient background subtraction.

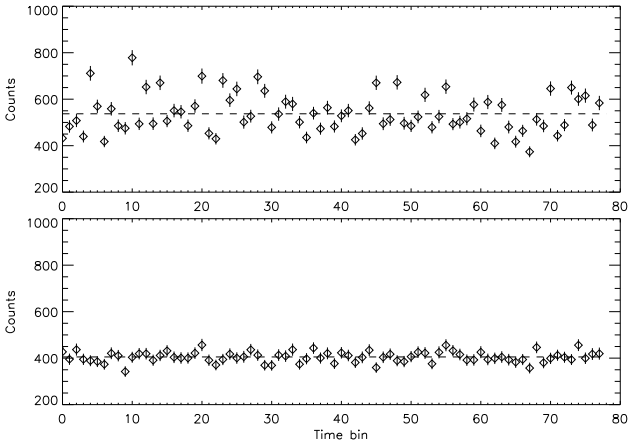

Fig. 4. Light curves of a sample of *photon by photon* data for PICsIT single events. Events are rebinned on 100s. Plotted errors are the expected Poisson uncertainties (1 σ). On the upper plot, the total light curve shows important flickering. This is not present when phosphorescence events are removed from the data (lower plot).

4. Effects of phosphorescence induced events

The PICsIT detector is found to show significant count-rate increase caused by *fake* events, induced by decay of phosphorescent states in the CsI crystals. These states are excited by passage of particles in the active body of the PICsIT detector, which occur at a rate $\sim$ 1000 times lower than the *normal* background rate. One *burst* of fake events can be produced by either the passage of a primary particle, or by a secondary shower (cascade) producing a track or other figure of well-defined spatial pattern (Segreto et al. 2003). All these counts are mostly detected at energies below $\sim$ 300 keV and can be easily recognized in *photon by photon* data, in which we have full timing in-

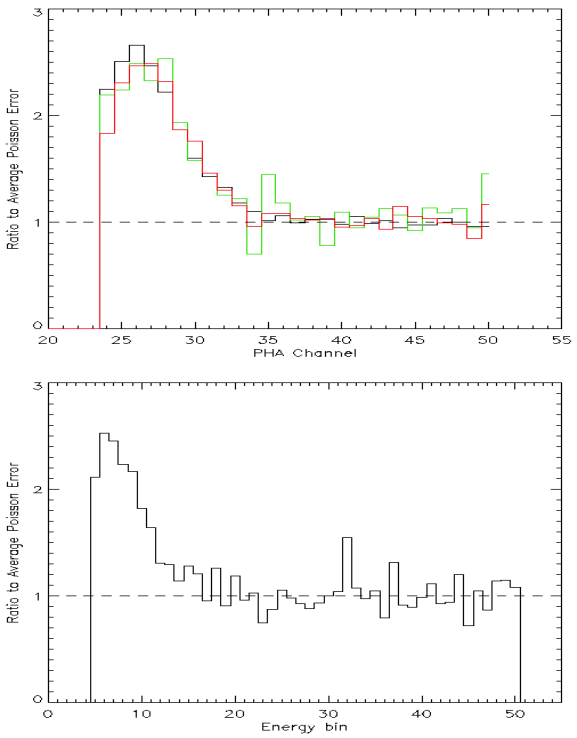

Fig. 5. The ratio of the observed standard deviation to the Poissonian expected value, as a function of energy bin, for PICsIT *photon by photon* data (top) and for PICsIT *spectral histograms* (bottom). The three curves in the upper panel refer to different integration times: 10s (black), 100s (red), 500s (green). The integration time of histograms is fixed to 2150s. In the upper panel, data are plotted against PHA channels, whilst in the lower panel, SI energy bins are used. Both X-axis scales are linear in energy, with a conversion factor ≈ 7 keV/bin. Due to the different offset, a value of 250 keV corresponds to abscissa values of 36 and 16 in the two plots, respectively.

formation. Since each individual passage of particles produces a relatively large number of these events, the count rate statistics is strongly modified. The two panels of Fig. 4 show the fluctuations of the summed count rate for 16 pixels of an ASIC, in the energy range 170-285 keV. On the upper plot, representing the total counts, the fluctuations are clearly non-Poissonian. Once the phosphorescence triggers are eliminated, the fluctuations are fairly compatible with Poissonian noise (lower panel). It is quite easy to recognize, by comparing the two plots, that some time bins are not affected at all by phosphorescence triggers. This effect can be quantified by computing the ratio, R, between the observed standard deviation of the counts and the Poisson statistical error, as a function of energy and for different integration times. In Fig. 5 (upper panel) are shown the values of R obtained from the same set of data (16 pixels, 8.2×10^4 s). From the figure, it is clearly seen that the loss of sensitivity per channel does not depend on integration time for $\Delta T \geq 10$s.

We have then investigated the effect of these fake events in *spectral imaging* data, which is the PICsIT standard mode of operation, using an empty field exposure (integration time: 2150s). As the background intensity always shows a long-term trend, expected values of rates were computed by a linear fit to the data, after selecting an interval of constant linear variation of 25 hours. For this test, we have used total count rates and verified that a large spreading of the values is also present in the energy channels below ≈ 250 keV (see Fig. 5, lower panel).

The ratio R changes significantly when rebinning in energy. For example, we estimate $R \approx 4.5$ and $R \approx 1.7$ for the energy bands 170-220 keV, and 220-280 keV respectively. These values are sensibly higher than the ones plotted in Fig. 5 for the single energy channels. This is actually expected, as each track produced by a particle leaves a number of phosphorescent counts which are widely distributed in energy, thus giving rise to highly correlated count rate fluctuations in different energy channels.

Finally, we investigated the spatial distribution of the fake events by using the *photon by photon* data. The images obtained in the energy band 170-285 keV clearly show that the non-uniformity in this range cannot be ascribed to the phosphorescence triggers (see Fig. 6).

5. Conclusions

Several effects which reduce the sensitivity of the imaging methods used by IBIS, especially in the PICsIT high energy layer have been described. Some of them are ascribed to image non-uniformity, and can be corrected by a large extent by a suitable flat-field. Some background components (namely, the delayed phosphorescence emission of the CsI crystals) are found to compromise the sensitivity in the energy range 180-250 keV, when IBIS is operated in its Standard Mode. Image non-uniformity problems are described in the framework of finding good methods for background subtraction. The presence of local systematic effects due to variable or unexpected behaviour of single pixels and/or ASICs is hampering the application of *standard* flat-field techniques. Present efforts are devoted to understanding/modelling this type of systematics, at the same time refining the already available methods of background correction.

Acknowledgements. The IBIS project is partially granted by Italian Space Agency (ASI). AJB is funded by PPARC grant GR/2002/00446.

References

Goldwurm, A., Goldoni, P., Gros, A., et al., 2001, Proc. 4th INTEGRAL Workshop, ESA-SP 459,497
Goldwurm, A., David, P., Foschini, L., et al., 2003, this volume
Hurley, K.C., 1978, A&A, 69, 313
Labanti, C., Di Cocco, G., Ferro, G., et al., 2003, A&A, this volume
Laurent, P., Limousin, O., Malaguti, G., et al., 2001, Proc. 4th INTEGRAL Workshop, ESA-SP 459,587
Lebrun, F., Leray, J.P., Lavocat, P., et al., 2003, A&A, this volume
Natalucci, L., Caroli, E., 1996, SPIE Vol.2806, 289
Quadrini, E.M., Bazzano, A., Bird, A.J., et al., 2003, A&A, this volume
Segreto, A., Labanti, C., Bazzano, A., et al., 2003, A&A, this volume
Stephen, J.B., Caroli, E., Malizia, A., et al., 2003, A&A, this volume

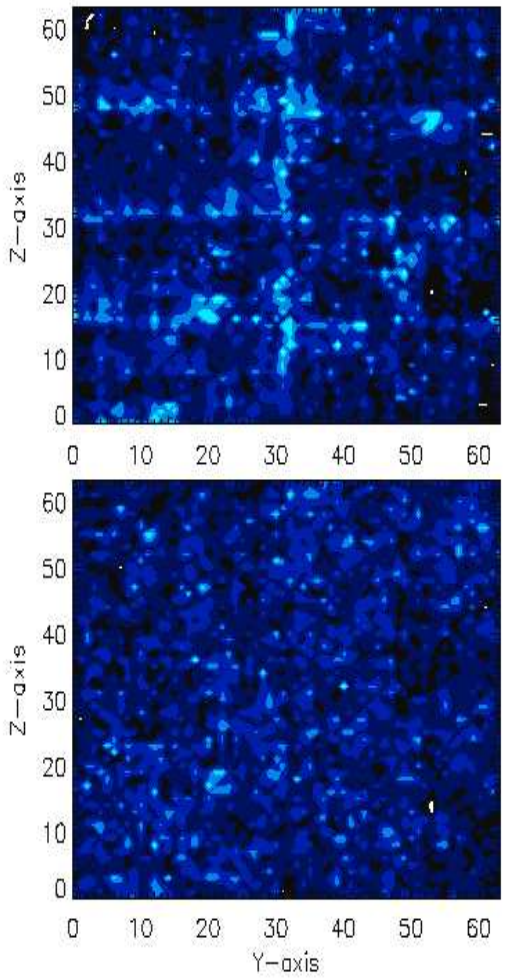

Fig. 6. The spatial distribution of normal background events in PICsIT (upper image), compared to that of phosphorescence triggers in the energy band 170-285 keV (lower image). The image axes are the same specified in Fig. 1.

Terrier, R., Lebrun, F., Bazzano, A., et al., 2003, A&A, this volume
Ubertini, P., Lebrun, F., Di Cocco, G., et al., 2003, A&A, this volume
Winkler, C., Courvoisier, T.J.-L., Di Cocco, G., et al., 2003, A&A, this volume